agriculture

MDPI

Article

Stability Control of the Agricultural Tractor-Trailer System in Saline Alkali Land: A Collaborative Trajectory Planning Approach

Guannan Lei [1], Shilong Zhou [2], Penghui Zhang [1], Fei Xie [3], Zihang Gao [1], Li Shuang [1], Yanyun Xue [4], Enjie Fan [4] and Zhenbo Xin [2,*]

[1] School of Mechanical Engineering, North University of China, Taiyuan 030051, China; guannanlei@bjfu.edu.cn (G.L.); 20230035@nuc.edu.cn (P.Z.); sz202202003@st.nuc.edu.cn (Z.G.); b20210206@st.nuc.edu.cn (L.S.)
[2] State Key Laboratory of Crop Biology, College of Agronomy, Shandong Agricultural University, Tai'an 271018, China; 2023110081@sdau.edu.cn
[3] Shanxian Huxi Institutes of Industrial Technology, Heze 274300, China; xf@hxiit.cn
[4] Chongqing Chang'an Wangjiang Industry Group Co., Ltd., Chongqing 401120, China; s202402032@st.nuc.edu.cn (Y.X.); 18600515748@casz.com (E.F.)
* Correspondence: 20220100@nuc.edu.cn; Tel.: +86-0351-3922102

Abstract: The design and industrial innovation of intelligent agricultural machinery and equipment for saline alkali land are important means for comprehensive management and capacity improvement of saline alkali land. The autonomous and unmanned agricultural tractor is the inevitable trend of the development of intelligent machinery and equipment in saline alkali land. As an underactuated system with non-holonomic constraints, the independent trajectory planning and lateral stability control of the tractor-trailer system (TTS) face challenges in saline alkali land. In this study, based on the nonlinear underactuation characteristics of the TTS and the law of passive trailer steering, a dual-trajectory collaborative control model was designed. By solving the TTS kinematic/dynamic state space, a nonlinear leading system that can generate the reference pose of a tractor-trailer was constructed. Based on the intrinsic property of the lateral deviation of the TTS, a collaborative trajectory prediction algorithm that satisfies the time domain and system constraints is proposed. Combining the dual-trajectory independent offset and lateral stability parameter of the TTS, an energy function optimization control parameter was constructed to balance the system trajectory tracking performance and lateral control stability. The experimental results showed good agreement between the predicted trailer trajectory and the collaborative control trajectory, with an average lateral error not exceeding 0.1 m and an average course angle error not exceeding 0.054 rad. This ensures that the dynamic controller designed around the tractor-trailer underactuation system can guarantee the smoothness of the trailer trajectory and the controlling stability of the tractor in saline alkali land.

Keywords: dual-trajectory collaborative planning; intelligent agricultural machinery; lateral stability control; saline alkali land; tractor-trailer system

Academic Editor: Kenshi Sakai

Received: 3 December 2024
Revised: 22 December 2024
Accepted: 27 December 2024
Published: 3 January 2025

Citation: Lei, G.; Zhou, S.; Zhang, P.; Xie, F.; Gao, Z.; Shuang, L.; Xue, Y.; Fan, E.; Xin, Z. Stability Control of the Agricultural Tractor-Trailer System in Saline Alkali Land: A Collaborative Trajectory Planning Approach. *Agriculture* **2025**, *15*, 100. https://doi.org/10.3390/agriculture15010100

1. Introduction

The tractor-trailer system (TTS), which is the most commonly used mechanical transportation equipment, has been employed in the comprehensive management of saline alkali land [1,2], agricultural product transshipment [3,4], and the research and design of

agricultural machinery [5,6]. Generally, the TTS consists of an autonomously controllable tractor and an unpowered trailer [7,8]. As such, the TTS is classified as an underactuated system, which represents a significant area of research in control theory, particularly regarding trajectory prediction and motion control [9,10]. Investigating the dynamic performance of the TTS based on non-holonomic constraints can provide a crucial foundation for future studies focused on the intelligent development and industrial innovation of agricultural machinery in saline alkali environments [11,12].

The balance between trajectory tracking and control stability is crucial for the safe operation of TTS [13]. In [14], Wen et al. developed a control strategy for unmanned spraying tasks to achieve effective path-tracking control of TTS in agricultural settings. This method enhances the efficiency of TTS spray path planning by combining reference trajectory presetting with a dual control strategy. In [15], the path planning problem for the TTS system was reformulated as a convex optimization problem using the "Farkas lemma". Integrating the constraints of the road environment and vehicle system into inequalities, a TTS motion planner was developed. In [16], the system's planning cost was comprehensively evaluated by creating an energy function equation that integrates TTS condition parameters such as energy consumption, force, and constrained condition. It provides a novel perspective for TTS system control. However, improvements are needed in the system's passability and adaptability, particularly when executing sharp turns [17–19].

In [20], a framework for road slope and mass estimation that accounts for changes in pitch angle was proposed. This framework designs a physically feasible neural network-based pitch angle estimator to assess the pitching effect in longitudinal acceleration sensor data. In [21], Zhou et al. implemented a steering-assist mechanism on the tractor. By actively adjusting the tractor's attitude, the system ensures accurate trajectory tracking. In [22], a TTS state-estimation algorithm was introduced, utilizing historical state information from the tractor. By combining TTS state estimation with real-time observations, the forecast trajectory was reconstructed and refined. In [23], the statistical results of passive steering angles were employed to model the motion dynamics of the TTS. Due to the low velocities involved, these studies primarily focus on the kinematic performance of the TTS [24].

Attempts have also been made to integrate TTS trajectory prediction with deep learning techniques. In [25], a gated recurrent unit was employed to calculate the heading angle, while an observer measures the hinge angle. Subsequently, motion estimation and error compensation are performed using a Kalman filter. This approach primarily focuses on the states of the tractor and trailer but pays insufficient attention to the perception and interaction between the TTS and the road. In [26], a machine learning framework based on TTS parameter statistics was developed to facilitate the prediction and guidance of system trajectories. However, this algorithm still requires a substantial amount of experimental data for effective training and validation [27].

Scholars have conducted extensive research on the auto-navigation strategies of the TTS [28–30]. However, there is limited research and development focused on TTS applications in saline alkali land farms [31–33]. Most studies primarily concentrate on the tracking accuracy of TTS under low-speed conditions [34,35]. In high-speed scenarios, these control strategies tend to overly emphasize the tracking performance of trailers along individual trajectories. Consequently, the trajectory of the trailer may become discontinuous and difficult to predict, which poses safety risks for overloaded TTS [36,37].

In this study, an intelligent control scheme for the agricultural tractor-trailer system, which is a typical underactuated multi-body system, is proposed. A dual-trajectory collaborative prediction strategy and a lateral error stability control method are introduced to address the stability control of the tractor-trailer system (TTS). The construction of the dynamic model under high-speed conditions is analyzed, and a solution to the leader-

follower consistency problem, considering discrete pose and velocity, is developed in the time domain. A lateral error evaluation and control scheme is designed by integrating high-speed and low-speed dual-branch structures. The main contributions of this study are as follows:

- Aiming to address the underactuated characteristics of the agricultural tractor-trailer system operating on saline alkali land, a kinematic/dynamic model was developed using the state-space representation of nonlinear autonomous systems with non-holonomic constraints. This model serves as a foundation for the discrete mathematical representation and computational analysis of the system's states;
- By integrating the development of a dynamic model with first-order discretization of the system in the time domain, we propose a dual-trajectory collaborative planning method for TTS. This approach clarifies the characteristics and behaviors of internal wheel difference (IWD) in underactuated TTS. Additionally, we present a solver designed to address the randomization of IWD errors and the unpredictability of trailer trajectories commonly encountered in traditional methods. Our dynamic analysis and state constraints, based on the collaborative trajectory algorithm, ensure predictable and quantifiable planning of trailer trajectories;
- A lateral error stabilization controller for a tractor-trailer system based on dual-trajectory collaborative planning is proposed. Unlike previous efforts, this control scheme fully considers the motion pattern and lateral state of the trailer in TTS. As a result, it effectively balances system stability with trajectory consistency.

2. State Space of the Tractor-Trailer System

This section introduces the construction scheme of the TTS kinematic/dynamics model. To achieve the closed-loop feedback performance for the TTS, a yaw plane model was established.

2.1. Observable and Controllable Model of the Tractor

In the construction of agricultural tractor-trailer engineering vehicles designed for saline alkali land, a rear-wheel-drive vehicle was utilized as the tractor, while the trailer was unpowered (as shown in Figure 1).

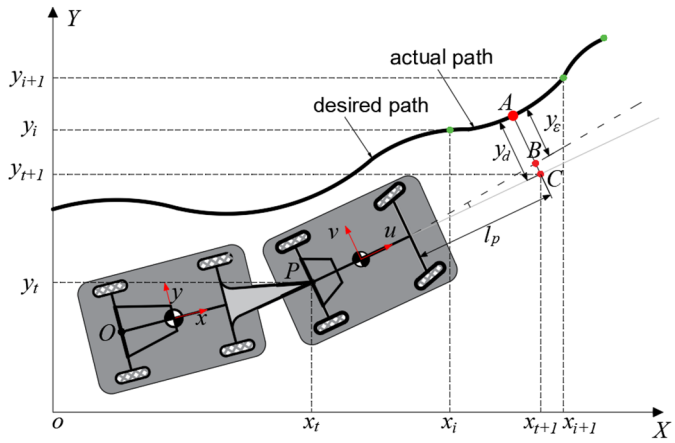

Figure 1. The tractor-trailer system maneuver geometry and instantaneous state diagram.

This study found that the kinematic performance of TTS is primarily investigated at low speeds [38]. However, as speed increases, dynamic characteristics become the main factor influencing the motion behavior of the TTS [39]. Therefore, a kinematic model was established in this study. To facilitate the solution of the system state, the midpoint of the

rear axles of the TTS (symbols P and O) was used as the reference point for calculating position coordinates.

$$y_\varepsilon = y_d - l_p v/u \tag{1}$$

Here, y_d is the error between the vehicle's position and the preset trajectory; y_ε is the distance between the preview result and the planned trajectory after adjusting the front wheel angle; v and u are orthogonal decomposition components of velocity in the vehicle's coordinate system, respectively; l_p is the preview distance.

The input of the control system in traditional driver systems can be abstracted as the state of motion of the system, which is uniquely determined by the yaw angle at certain speeds. The solution for the heading-angle control quantity is as follows:

$$G_m\, y_\varepsilon\, \Delta T_s = \delta_1(t) \tag{2}$$

G_m is the gain ratio, and ΔT_s is the delay time of the mechanical unit. Equation (3) can be obtained from the Laplace transform:

$$G_m\, y_\varepsilon(s)\, e^{-\Delta Ts} = \delta_1(s) \tag{3}$$

The Taylor series was used to expand the low-order approximate solution equation as follows:

$$\delta_1(s) + \Delta T_s s \delta_1(s) = G_m y_\varepsilon(s) \tag{4}$$

An inverse Laplace transform was performed to obtain the first-order differential equation for the steering input.

$$\dot{\delta}_1(t) = (G_m y_\varepsilon(t) - \delta_1(t))/\Delta T_s \tag{5}$$

This is a mathematical description of the control quantity of a tractor. Owing to the small high-order error term and the fact that the calculation results were dynamically updated and covered, the high-order term can be ignored.

2.2. The Tractor-Trailer System Kinematic Model

In general, the inputs to a vehicle system can be abstracted as direction and speed controls. Therefore, the TTS developed in this study is a planar model that ignores the influencing factors of the vehicle system, such as pitch jump and wind resistance in all directions under actual working conditions. The heading angle and speed of the system are both observable and controllable, and the phenomenon of vehicle-body folding does not occur.

The mathematical expression of the system's motion state is presented in Equation (6) (for the kinematics equation, some parameters in Figure 2 are redundant):

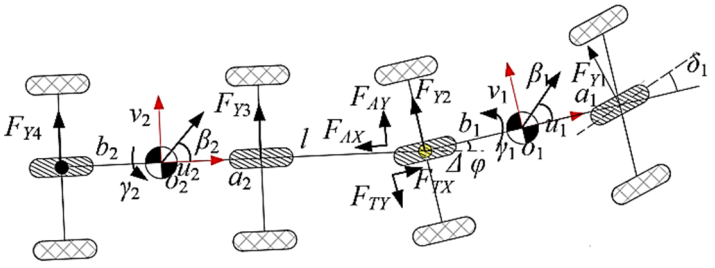

Figure 2. The tractor-trailer system dynamic analysis and modeling.

$$q = \left[x_j, y_j, \delta_1, \delta_2\right]^T \tag{6}$$

(x_j, y_j) is the coordinate of the point O; δ_1 and δ_2 are the steering angles of the tractor and the trailer, respectively. The TTS status can be fully represented by the above parameters and known parameters:

$$x_i = x_j + (a_2 + b_2 + l)cos\delta_2 - Lcos\delta_1 \tag{7}$$

$$y_i = y_j + (a_2 + b_2 + l)sin\delta_2 - Lsin\delta_1 \tag{8}$$

The coordinates of point P $(x_j^{'}, y_j^{'})$ can be updated and obtained:

$$x_j^{'} = \Delta s_j A_1 + x_j \tag{9}$$

$$y_j^{'} = \Delta s_j A_2 + y_j \tag{10}$$

A_1 and A_2 are the parameter matrix, and Δs_j is the trailer's discrete step.

2.3. The Tractor-Trailer System Dynamics Model

Based on the underactuation characteristics of the TTS, the linear yaw plane model for the dynamics was further developed based on the transient model (as shown in Figure 2).

$$m_1(\dot{v}_1 + \gamma_1 u_1) = F_{Y1}cos\delta_1 + F_{Y2} + F_{AY} \tag{11}$$

$$I_{Z1}\dot{\gamma}_1 = a_1 F_{Y1}cos\delta_1 - b_1 F_{Y2} - b_1 F_{AY} \tag{12}$$

$$m_2(\dot{v}_2 + \gamma_2 u_2) = F_{Y3} + F_{Y4} - F_{TY} \tag{13}$$

$$I_{Z2}\dot{\gamma}_2 = a_2 F_{Y3} - b_2 F_{Y4} - (a_2 + l)F_{TY} \tag{14}$$

In Equations (11)–(14), m_i is the mass of the tractor or the trailer; I_{zi} represents the moment of inertia; v_i is the lateral velocity; u_i is the longitudinal velocity; γ_i is the angular velocity at which the tractor or the trailer rotates around the center of mass. F_{Y1}, F_{Y2}, F_{Y3}, and F_{Y4} are the lateral forces of the ground against the tire. F_{AX}, F_{AY}, F_{TY}, and F_{TX} are the action and reaction force (through orthogonal decomposition) caused by the tow arm. a_i and b_i are the length from the front-axle center and the rear-axle center to the center of gravity of the tractor or the trailer. δ_i is the steering angles of the TTS. Among them, i = 1, 2.

Based on the longitudinal linear tire model, the lateral force exerted by the ground on the tires can be expressed as follows:

$$F_{Y1} = \left(\lambda_1 + \frac{a_1\gamma_1}{u_1} - \delta_1\right)C_1 \tag{15}$$

$$F_{Y2} = \left(\lambda_1 - \frac{b_1\gamma_1}{u_1}\right)C_2 \tag{16}$$

$$F_{Y3} = \left(\lambda_2 + \frac{a_2\gamma_2}{u_2} - \delta_3\right)C_3 \tag{17}$$

$$F_{Y4} = \left(\lambda_2 - \frac{b_2\gamma_2}{u_2}\right)C_4 \tag{18}$$

where C_i (i = 1, 2, 3, 4) is the rolling resistance coefficient between the tire and the ground, and the driver's perspective is used as the benchmark to unify the vehicle coordinate

system. According to the tool manual, C_i = 0.035 [40]. The TTS is linked by articulation, and the mechanical constraint equation between the two is expressed as follows:

$$F_{Ax} = F_{Tx}cos\Delta\varphi - F_{Ty}sin\Delta\varphi \tag{19}$$

$$F_{Ay} = -F_{Tx}sin\Delta\varphi - F_{Ty}cos\Delta\varphi \tag{20}$$

The kinematic constraint equation for the TTS is as follows:

$$u_2 = u_1cos\Delta\varphi - [v_1 - \gamma_1 \cdot (b_1 + c)]sin\Delta\varphi \tag{21}$$

$$v_2 + (a_2 + d)\gamma_2 = u_1\Delta\varphi + v_1 - \gamma_1 \cdot (b_1 + c) \tag{22}$$

The instantaneous state of the system can be regarded as uniform speed, and the following equation can be written:

$$\lambda_2 = \lambda_1 - (b_1 + c)\gamma_1/u + (a_2 + d)\gamma_1/u \tag{23}$$

In addition, the following relationship can be obtained between γ_1 and γ_2:

$$\gamma_1 - \gamma_2 = \Delta\dot{\varphi} \tag{24}$$

Through (19)–(24), $x = [\lambda_1, \gamma_1, \gamma_2, \Delta\varphi]$. The TTS state equations can thus be expressed:

$$\dot{x} = [A\ B_1 B_3][x\ \delta_1 \delta_2]^T \tag{25}$$

Details of each matrix definition of (25) are given in Appendix A.

3. Lateral Stabilizer Based on Dual-Trajectory Prediction

For the nonlinear control requirements of agricultural tractor-trailer systems in saline alkali land, this section introduces a lateral stabilization controller that utilizes dual-trajectory planning. The design of this controller necessitates a balance between the lateral control stability of the TTS with the lateral regression error during steady-state maneuvers.

3.1. Dual-Trajectory Collaborative Planning

Based on the TTS, the dual-trajectory collaborative algorithm was designed as shown in Algorithm 1. The parameters required for system input and initialization include the parameters of the TTS, global coordinates, attitude information, and the reference trajectory. The algorithm outputs the trailer trajectory, the system pose, and control parameters.

The position of the TTS was calculated using the numerical solution of the dynamic model. As the TTS was driven, the status parameters for the current and subsequent steps were recorded. The system parameters follow the rule of "first-in, first-out" and iterate over time. The updated process of the TTS state was discretized from the time scale, and the iteration and sampling process was as follows.

3.2. Design of Lateral Stability Controller

Based on the TTS state, we further optimized the model control strategy. In traditional studies, the tracking performance of the tractor and the trailer in the TTS has been uniformly evaluated based on specific paths. In contrast to conventional methods, the establishment of the TTS and the prediction of dual-collaborative trajectories offer a more reliable foundation for calculating the path-following lateral offset (PFLO). PFLO refers to the lateral deviation between each independent vehicle body (tractor and trailer) and their

respective trajectories. Here, the PFLO of each vehicle body was calculated independently and evaluated comprehensively.

Algorithm 1 The Dual-collaborative trajectory planning algorithm core

Inputs: Parameter customization of the TTWR platform (a_1, b_1, a_2, b_2, I_{Z1}, I_{Z2}), the initial position of TTWR (x_i, y_i), (x_j, y_j), the traction arm length l, the maximum yaw angle of the tractor δ_{max}, and the discretized initial path.
Outputs: The Dual-collaborative trajectory path V and the state variable $x = [\lambda_1 \ \ \gamma_1 \ \ \gamma_2 \ \ \Delta\varphi]$
1:System Initialization: the base path $Path_I$ = {P_{set} [0], P_{set} [1], $\cdots$, P_{set}[end]}, the trailer trajectory $Path_J$ = {$NULL$}, the Dual-collaborativetrajectory $Path$ = {$Path_I$, $Path_J$}, the initial heading angle δ_1, δ_2
2:**If** P_{set} [0] $\neq$ P_{set}[end] or Distance > 0.03
3: **While** Distance > 0.03 m **do**
4: Calculate the current position of the tractor and trailer O and P
5: Update the step length Δs_i, $\Delta s_j \rightarrow uT$ and the curvature of the tractor ρ_i, ρ_j
6: Update the coordinates of tractor (x_i, y_i), the new heading angle of tractor δ_1, the new
yaw angle of tractor δ_2
7: Calculate the speed γ_i (i = 1,2) of the tractor or the trailer rotates around the center of mass O_i (i = 1,2), the sideslip λ_i (i = 1,2) angle and update
8: Update the trailer coordinates (x_j, y_j), the trailer new heading angle δ_1, δ_2
9: Calculate the deviation e_1, e_2
10: **If** the distance between the trailer and the road boundary ≤ 0
11: Update the $Path_I$
12: **Break**
13: Save the current position $Path_J$ = {P_{set} [0], P_{set} [1], $\cdots$, $P_{set}[k-1]$, $P_{set}[k]$}
14:**else**
15: Reach the end point
16: Generate the collaborative trajectory path V = {$Path_I$, $Path_J$}
Where Distance is the distance between the current position of the tractor and the end point, e_1 and e_2 are the deviation between the tractor track and the trailer track.

To enhance improve the steady-state characteristics of TTS under high-speed conditions, the lateral acceleration was considered another control target for the TTS. The RWA is the ratio of the trailer's lateral acceleration to that of the tractor, and it is closely related to lateral stability. In this study, for convenience of calculation, the reference point of the RWA was deployed in the rear axle of the TTS. The mathematical description of RWA = $\left[a_{y1}, a_{y2}\right]^T$ is as follows:

$$\begin{bmatrix} a_{y1} \\ a_{y2} \end{bmatrix} = \begin{bmatrix} M_1 & F_1 \\ M_2 & F_2 \end{bmatrix} \begin{bmatrix} \dot{x} \\ x \end{bmatrix} \tag{26}$$

where M_1 = [u, 0, 0, 0]; F_1 = [0, u, 0, 0]; M_2 = [u, $-(b_1 + c)$, $-(a_2 + d)$, 0]; and F_2 = [0, 0, u, 0].

The steering angle is determined by the error between the system's attitude and the predetermined trajectory. Therefore, Equation (27) can be discretized:

$$\begin{bmatrix} a_{y1}(k) \\ a_{y2}(k) \end{bmatrix} = \begin{bmatrix} M_1 A + F_1 & M_1 \\ M_2 A + F_2 & M_2 \end{bmatrix} \begin{bmatrix} x(k) \\ B_3 \delta_2(k) \end{bmatrix} \tag{27}$$

Based on PFLO and RWA, the lateral steady-state control and evaluation function *Co* of the system can be expressed as follows:

$$Co(k) = \sum_{k=1}^{\infty} \left\| V^T(k) Q' V(k) + 2V^T(k) U' \delta_2(k) + \delta_2^T R' \delta_2 \right\|^2 \tag{28}$$

$$Q' = L_1^T (M_1 A + F_1)^T W_{22} (M_1 A + F_1) L_1 + L^T W_{21} L + L_1^T (M_2 A + F_2)^T W_{23} (M_2 A + F_2) L_1 \tag{29}$$

$$U' = L_1^T (M_2 A + F_2)^T W_{23} (M_2 A + F_2) B_3 + L_1^T \left(M_1 A + F_1 \right)^T W_{22} M_1 B_3 \tag{30}$$

$$R' = \left(M_2 B_3 \right)^T W_{23} (M_2 B_3) + (M_1 B_3)^T W_{22} M_1 B_3 + W_{24} \tag{31}$$

W_{21} is the weight of the lateral following error PFLO; W_{22} and W_{23} are the lateral acceleration weights of the tractor and the trailer; W_{24} is the weight of the yaw angle of the trailer; $L_1 = [I_{4\times4} O_{4\times(2n+2)}]$, $I_{4\times4}$ is 4×4 identity matrix; and $O_{4\times(2n+2)}$ is $4 \times (2n + 2)$ null matrix.

$$G_{com} = \dot{\mathcal{L}}(Co(k)) \tag{32}$$

The gain matrix G_{com} can be acquired using the Lagrange extremum method to minimize the cost function *Co*. The optimized TTS steering angle can be expressed as follows:

$$\delta' 1_{com} = G_{com} V(k) \tag{33}$$

To illustrate the implementation process of the dual-trajectory collaborative control strategy, Figure 3 presents a block diagram of the implementation. Based on the observations of the actual and expected poses of the TTS, deviations e_1 and e_2 between the actual and desired paths were estimated. Then, the deviation value e_1 and e_2 were fed back to the control model to obtain the steering angle δ_1. Using δ_1 as the input the cost function, the modified optimal solution δ_{1com} was calculated according to the collaborative trajectory prediction algorithm and the PFLO lateral stability controller. As the TTS traverses a step, combined with the input δ'_{1com} from the previous step, the new state information for the TTS was updated, and the system was solved for the new δ_1 again. Thus, a closed-loop control process was achieved. In addition, considering the rollover risk assessment at high speed, an empirical maximum adjustment of 10° for the yaw angle was introduced as a constraint. In this study, a speed of 30 km/h was used as the threshold between high speed and low speed. When the system exceeds 30 km/h, it is classified as high speed, and when it falls below 30 km/h, it is classified as low speed.

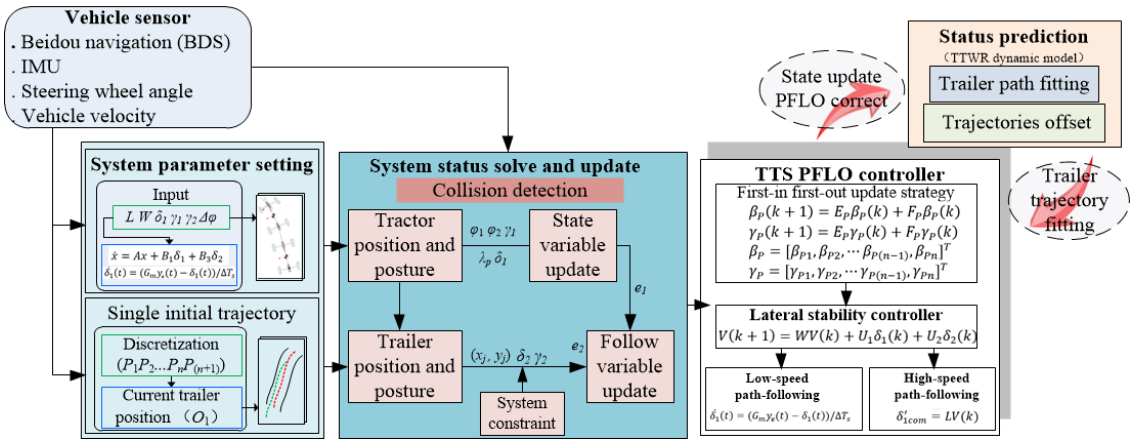

Figure 3. Control block diagram of dual-trajectory collaborative strategy based on the TTS dynamic model.

4. Experimental Results and Discussion

4.1. Construction of the Tractor-Trailer System Experimental System

Based on the saline alkali land agricultural TTS, an underactuated intelligent experimental platform was developed, as shown in Figure 4. Similar in structure to the agricultural TTS, the intelligent experimental platform consists of two components: an autonomously controllable tractor and a non-powered trailer. The tractor provides the power for the system, and the trailer provides the load capacity for the system. Its configuration is as follows: The size of the tractor is 970 mm × 680 mm × 400 mm. The size of the trailer is the same as the tractor. The traction arm (the distance between the tractor and the trailer) is 0.4 m. The configuration of the TTS industrial control computer is as follows: The system is configured with Linux 20.04 and ROS-noetic. The motherboard is equipped with an Intel i7-13700 K CPU and 256 GB of RAM.

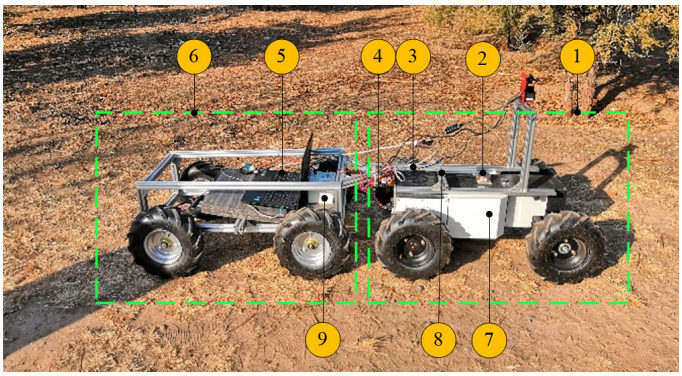

Figure 4. Self-developed tractor-trailer intelligent navigation experimental platform: 1, Tractor module; 2, IMU; 3, traction arm; 4, CAN2USB; 5, epigynous computer (PC); 6, trailer module; 7, electrical bin; 8, hinge point; 9, vehicle power supply.

In order to ensure accurate observation of the position and orientation of the TTS system, the system integrated the "Beidou Navigation Satellite System (BDS) + Inertial Measurement Units (IMU)" module. The IMU model used is the RION TL-740D. The architecture for signal acquisition, storage, and sharing is integrated into the software system. Channels and nodes for signal publication and subscription are established for each sensor. Specifically, the measurement of the steering wheel angle was achieved through the collaboration of the steering gear and the angle encoder, while speed feedback was obtained from both the GPS unit and the IMU. This setup provides crucial feedback and reference information for the system. The TTS has a carrying capacity of no less than 100 kg, and the maximum yaw angle of the tractor is 40°.

4.2. Collaborative Trajectory Planning of the Tractor-Trailer System

During the experiment, the initial path was loaded into the TTS as a BDS, which served as part of the initial system input. Figure 5 illustrates the dual-trajectory collaborative planning experiment based on TTS-KM (the tractor-trailer system kinematic modeling) and TTS-DM (the tractor-trailer system dynamic modeling). The curve lane models corresponding to the four graphs were 120° (Figure 5a), 90° (Figure 5b), 60° (Figure 5c), and 180° (Figure 5d), respectively, with a turning radius of 4.8 m. The blue curve represents the boundary of the road; the thick yellow curve indicates the reference trajectory. The green curve is generated by the TTS-KM at low speed. The fine yellow curve illustrates the trajectory predicted using the dynamic model proposed in this study. It is important to note that, for the sake of clarity and calculation, both the green and thick yellow curves were fitted based on the motion trajectory of the left rear wheel of the trailer rather than the midpoint of the rear axle or the center of gravity.

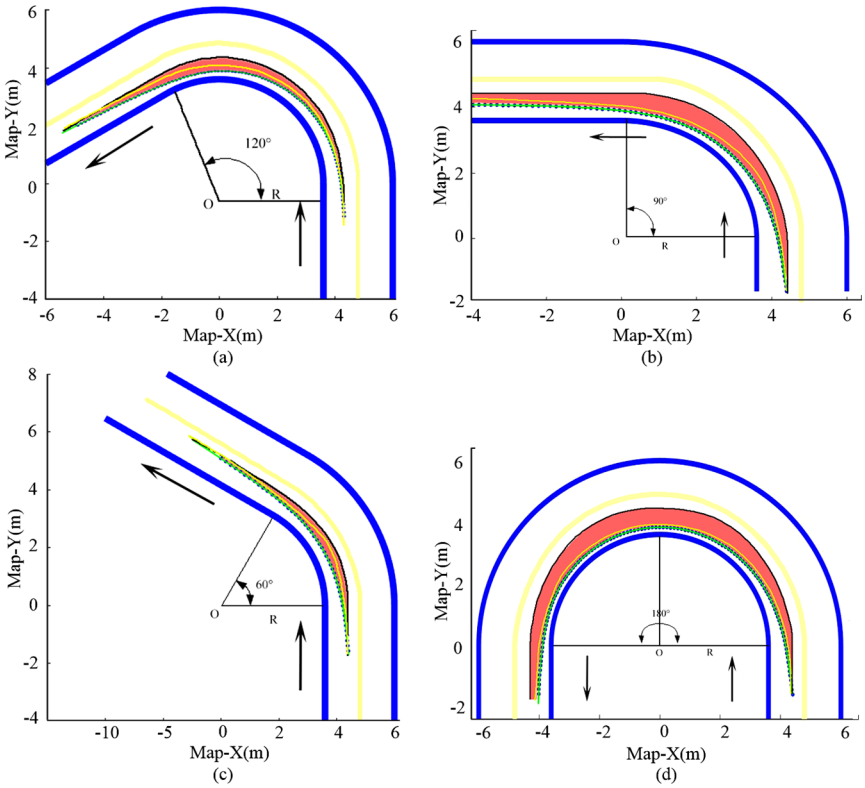

Figure 5. Dual−trajectory collaborative planning experiment based on TTS−KM and TTS−DM.

As illustrated in Figure 5, the fine yellow curve does not precisely align with the green curve and is generally situated between the green and black curves. The system exhibits improved longitudinal stability and maintenance performance when the TTS operates at high speeds. However, the fine yellow and green curves are relatively close to each other. This proximity occurs because a larger turning angle amplifies the influence of the hinge point on the lateral traction of the trailer, resulting in a more pronounced lateral offset motion. It is evident that, regardless of whether the system is operating at high or low speeds, the lateral offset of the trailer remains constrained within a specific range, defined by upper and lower limits. Additionally, a comparison of the predicted trajectories from both methods mutually confirms the objectivity and predictability of the IWD phenomenon in the TTS.

4.3. Analysis of Lateral Offset Law of Trailer

In order to enhance the accuracy and intuitiveness of the inductive results, several additional groups of experiments were conducted. The results of the trailer's lateral migration during these experiments were statistically presented (as shown in Figure 6). The experiments adhered to the principle of controlling variables. With the exception of the black curve, the turning angle for all experiments was set at 180°, while only the turning radius was varied.

The curve depicted in Figure 6 was divided into three regions labeled I, II, and III, which correspond to the three stages of the lateral offset of the trailer. Region I is the stage of rapid increase in the trailer's lateral offset. During this phase, the tractor begins to enter the curve, and the trailer gradually follows suit, influenced by the tractor's traction. This traction effect is primarily reflected in its impact on the trailer's longitudinal speed. Subsequently, the system enters Region II. At this stage, the TTS completely enters the curve, and the gradient of the curve decreases; however, the lateral offset of the trailer continues to increase, ultimately reaching its maximum value. In Region III, the lateral

offset of the trailer decreases rapidly. During this phase, the tractor starts to exit the bend, and the trailer's trajectory gradually converges with that of the tractor until they overlap.

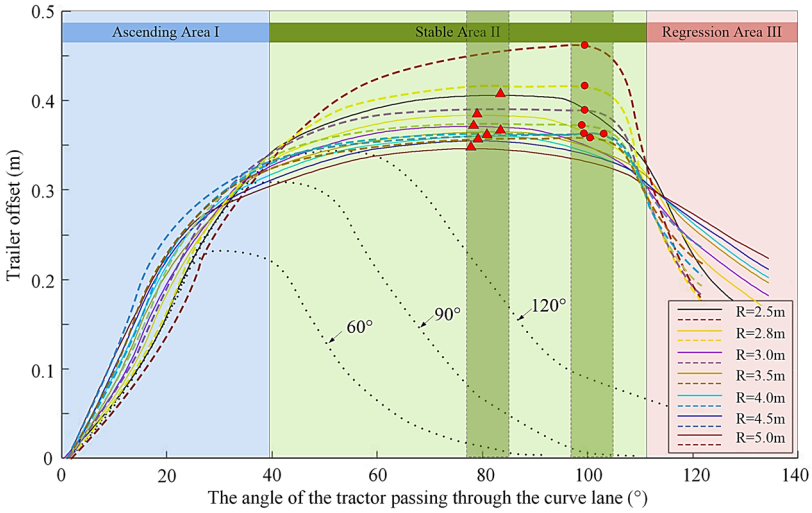

Figure 6. Variation curves of trailer lateral offset when the tractor-trailer system is traveling on 180° curved lanes with different turning radii.

In Figure 6, the dashed line corresponds to the results of the TTS-KM. The solid line is the results of the TTS-DM. The figure clearly illustrates that, for a specific turning angle of 180°, a smaller turning radius leads to a larger extreme value of the curve. The red triangles and red circles indicate the maximum positions of each curve, which represent the maximum lateral offset. At the 180° curve, the maximum offset of the trailer occurs (with TTS-DM) within the interval of 77–86° when entering the curve (dark-green interval range). In contrast with TTS-KM, the maximum offset (the extremum point) occurs in a range from 96° to 105°. This discrepancy may arise from two factors. First, due to the high speed of the tractor, the direction of the traction force changes rapidly during the turning process, causing the longitudinal force acting on the tractor to be quickly transformed into a lateral component after decomposition. Second, during the calculation process, the high speed causes the preview point to move forward, resulting in the maximum lateral deviation occurring earlier. The prediction results confirm that the trailer offset phenomenon is an intrinsic characteristic of the system and can be accurately predicted.

In addition, we took the black solid line as an example (with a turning radius of 2.5 m and a turning angle of 180°). We maintained the turning radius at 2.5 m while varying the turning angles to 60°, 90°, and 120° (represented by three dotted lines). These variations illustrate that, when the turning radius is fixed, a smaller turning angle results in reduced lateral deviation and a lower extreme value point.

4.4. Lateral Stability Control Results

Based on the above experiments, the algorithm in this study was preliminarily validated. Subsequently, the algorithm was implemented on our TTS experimental platform to further assess its engineering feasibility. As illustrated in Figure 7, the test results of the prototype were compared and analyzed against the predicted trajectory. The dotted magenta lines represent the preset reference trajectories. The cyan curve depicts the trajectory predicted by the algorithm. The black and green curves represent the actual running track at low and high speeds, respectively. It should be noted that, aside from the magenta curve, the remaining curves describe the trajectory of the trailer. The trajectory was determined using an embedded BDS-RTK module with a sampling frequency of 200 Hz.

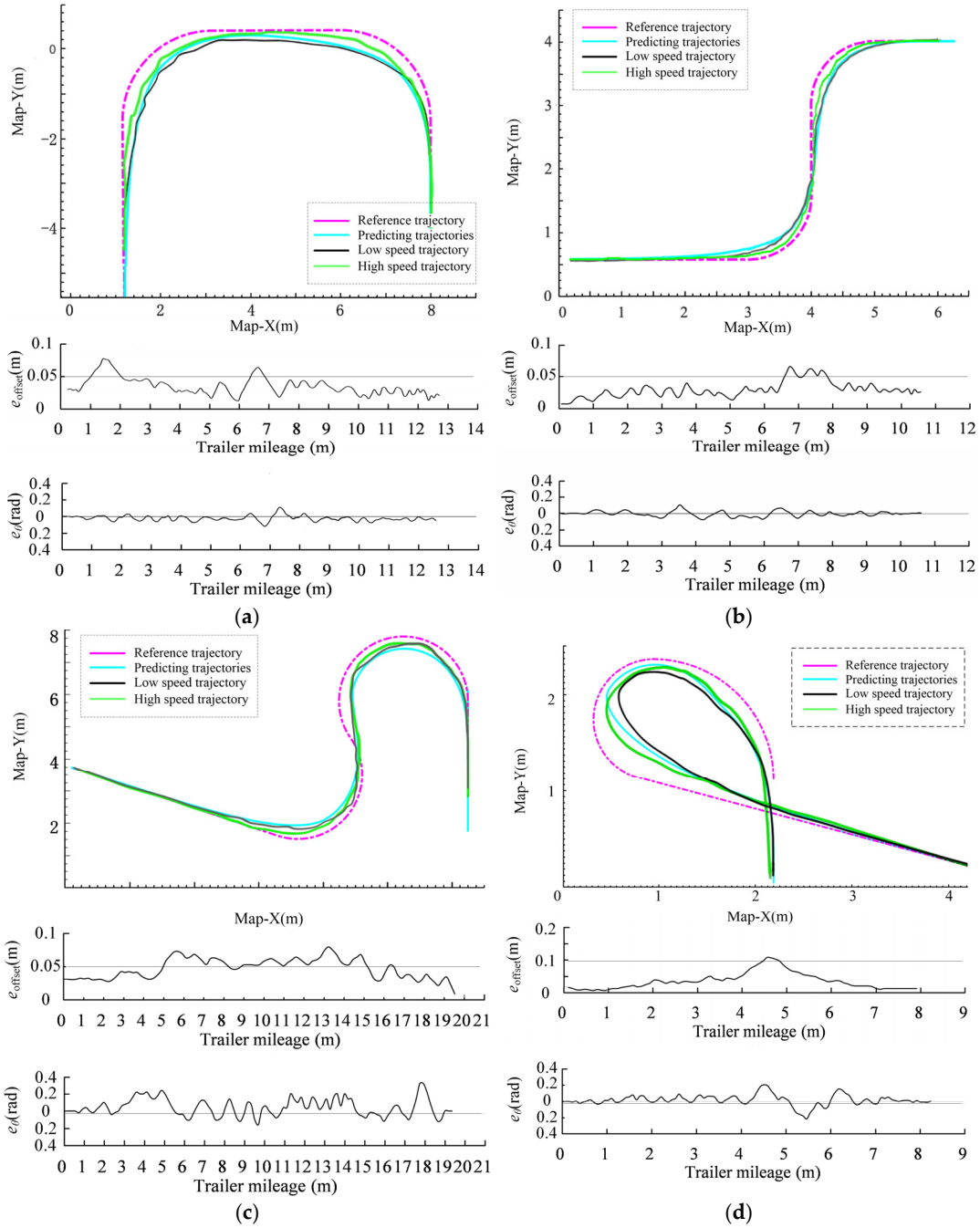

Figure 7. Trajectory prediction and tracking control experiments under different curves.

It is evident that, although the black and cyan curves demonstrate greater consistency, the trajectory of the trailer can be positioned between the predicted curve and the reference path, adequately meeting the tracking and control requirements. The green curve is closer to the magenta curve, indicating that the trailer's lateral tracking performance is superior at high speeds compared to low speeds. This observation can be attributed to two factors: First, the small turning radius set is near the minimum turning radius of the TTS, causing the trailer's predicted trajectory under limit conditions to closely resemble that of low-speed conditions. Second, relative to the ground, the trailer inevitably exhibits a slight amount of lateral sliding toward the magenta curve. Under conditions of sufficient friction, this minor lateral sliding of the trailer remains controllable.

In Figure 7a–c, the curves of e_{offset} show the variation trend of the lateral offset of the trailer during driving, where the x-axis is the mileage. The y-axis represents the error

between the lateral offset and the predicted trajectory. The fluctuation trends of the actual heading angle of the trailer are shown with e_θ. As can be seen, the deviation between the algorithm proposed in this study and the actual trajectory of the trailer is less than 0.1 m. The deviation between course angles usually does not exceed 0.2 rad.

In Figure 7d, we attempt to operate the Ackerman chassis at a high speed while maintaining a minimum turning radius of approximately 1.5 m and a speed of 18 km/h. For safety reasons, this speed was reduced compared to the previous three-group experiment. This test represented an extreme condition. There was a notable discrepancy between the actual motion trajectory under both low- and high-speed conditions and the predicted trajectory. The tractor and trailer appeared to fold while in motion. In fact, during the movement of the TTS, the risk of vehicle-body folding or rollover easily occurs on such roads at high speeds and must be avoided. According to the statistical results, the average offset was approximately 0.075 m (no more than 10 cm). For the heading angle of the trailer, the average offset was 0.032 rad, and the max offset was less than 0.2 rad.

4.5. Tracking Control Effectiveness Evaluation

To further illustrate the impact of control on the lateral steady state of the TTS, additional tracking and control experiments were conducted in saline alkali land farms. The experimental sites included the Guanxian Salt Alkali Land Experimental Field and the Wudi Salt Alkali Land Experimental Base of Shandong Agricultural University in Shandong Province, China. The roads in the saline alkali land are all dry and compacted, and the vehicles used are equipped with cross-country tread-pattern tires, which provide excellent friction and traction between the road and the tires. Consequently, based on the rolling resistance coefficient table, a value of $C_i = 0.035$ was selected for Equations (15)–(18). As illustrated in Figure 8, six experimental roads were chosen within the saline alkali land farm.

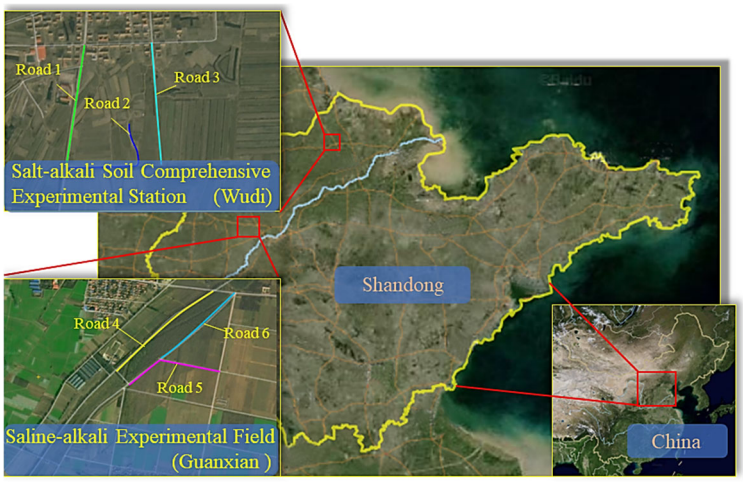

Figure 8. Salt-alkali land experimental base of Shandong Agricultural University.

To ensure the rigor of the experiment and the practicality of the algorithm, three conventional algorithms (PID, LQR, and Kalman), the proposed TTS-KM, and the TTS-DM were selected for comparison. As listed in Table 1, six indicators were used to systematically evaluate the tracking and control effects of the TTS. Max e_{off} represents the maximum deviation, mean e_{off} is the average deviation, and the standard deviation e_{off} represents the discrete deviation of the trailer during driving. Max e_θ represents the maximum heading angle deviation; mean e_θ represents the average heading angle deviation; and standard deviation e_θ represents the heading angle fluctuation of the tractor during driving. These two standard deviations (standard deviation e_{off} and standard deviation e_θ) can effectively measure the stability of TTS.

Table 1. Comparison of control results of TTS in saline alkali farmland road.

Number	Algorithm	PID	LQR	Kalman	TTS-KM	TTS-DM
Road 1	Max e_{off} (m)	0.586	0.214	0.183	0.125	0.112
	Mean e_{off} (m)	0.319	0.151	0.134	0.071	0.083
	Standard deviation e_{off}	0.032	0.106	0.100	0.016	0.009
	Max e_{θ} (rad)	0.490	0.292	0.287	0.279	0.275
	Mean e_{θ} (rad)	0.227	0.097	0.105	0.061	0.046
	Standard deviation e_{θ} (rad)	0.029	0.046	0.043	0.010	0.006
Road 2	Max e_{off} (m)	0.663	0.386	0.209	0.145	0.134
	Mean e_{off} (m)	0.405	0.167	0.152	0.092	0.098
	Standard deviation e_{off}	0.045	0.168	0.124	0.031	0.014
	Max e_{θ} (rad)	0.501	0.254	0.249	0.232	0.229
	Mean e_{θ} (rad)	0.254	0.153	0.125	0.058	0.054
	Standard deviation e_{θ} (rad)	0.035	0.043	0.042	0.019	0.009
Road 3	Max e_{off} (m)	0.527	0.389	0.248	0.119	0.149
	Mean e_{off} (m)	0.346	0.171	0.167	0.105	0.093
	Standard deviation e_{off}	0.051	0.105	0.103	0.045	0.035
	Max e_{θ} (rad)	0.357	0.261	0.253	0.238	0.210
	Mean e_{θ} (rad)	0.227	0.134	0.105	0.073	0.046
	Standard deviation e_{θ} (rad)	0.031	0.035	0.037	0.021	0.012
Road 4	Max e_{off} (m)	0.601	0.341	0.261	0.149	0.127
	Mean e_{off} (m)	0.378	0.164	0.158	0.112	0.083
	Standard deviation e_{off}	0.053	0.106	0.098	0.024	0.012
	Max e_{θ} (rad)	0.385	0.292	0.287	0.275	0.278
	Mean e_{θ} (rad)	0.198	0.162	0.112	0.068	0.049
	Standard deviation e_{θ} (rad)	0.036	0.046	0.041	0.023	0.011
Road 5	Max e_{off} (m)	0.532	0.354	0.240	0.183	0.142
	Mean e_{off} (m)	0.331	0.184	0.163	0.094	0.074
	Standard deviation e_{off}	0.048	0.126	0.115	0.051	0.034
	Max e_{θ} (rad)	0.512	0.238	0.199	0.198	0.185
	Mean e_{θ} (rad)	0.263	0.201	0.130	0.071	0.039
	Standard deviation e_{θ} (rad)	0.040	0.051	0.047	0.018	0.015
Road 6	Max e_{off} (m)	0.485	0.287	0.191	0.143	0.116
	Mean e_{off} (m)	0.278	0.201	0.140	0.083	0.078
	Standard deviation e_{off}	0.172	0.131	0.121	0.035	0.030
	Max e_{θ} (rad)	0.040	0.204	0.187	0.175	0.172
	Mean e_{θ} (rad)	0.186	0.124	0.100	0.058	0.043
	Standard deviation e_{θ} (rad)	0.035	0.054	0.031	0.012	0.011

In general, conventional tracking control methods such as PID, LQR, and Kalman utilize a single path as the reference trajectory for the TTS. During the experiment, the PID controller strictly adhered to the predetermined trajectory as the tracking path for the trailer. Statistical results indicate that the lateral deviation and stability control of the trailer outperform those achieved by the LQR and Kalman algorithms. However, this performance comes at the expense of the tractor's control effectiveness, as evidenced by the largest values of e_{off} and e_{θ} among the five methods evaluated. Consequently, in subsequent experiments, both the LQR and Kalman controllers aimed to distribute the tractor and trailer trajectories as evenly as possible on either side of the reference trajectory to achieve a balance between control and tracking performance within the system.

Compared to the PID controller, the lateral offset was controlled to a certain extent; however, the heading angle between the tractor and trailer exhibited significant fluctuations. This indicates that the tractor has made considerable compromises in control stability to

ensure effective trailer tracking. While large positional deviations can be corrected through adjustments, frequent modifications to the heading angle may introduce unknown risks. Therefore, this type of operation should be avoided under high-speed conditions.

In this study, due to the intrinsic properties of the TTS, the tractor and trailer do not overlap during turns. However, the trailer's trajectory can be reasonably predicted and planned under certain conditions. The two algorithms (TTS-KM and TTS-DM) consider both the tractor and trailer. The results indicate that the tracking and control outcomes were significantly optimized and improved. In six road experiments, the max e_{off} of the system did not exceed 0.2 m, and the max e_{θ} did not exceed 0.28 radians. The mean e_{off} and the mean e_{θ} decreased by at least one-third. Notably, the two standard deviation metrics decreased by more than two-thirds compared to conventional control methods. Furthermore, the proposed TTS-DM slightly outperformed the kinematic model at high speeds in terms of the two standard deviations. This suggests that the lateral control stability of the kinematic model was enhanced, which is crucial for the high speed.

In fact, even empirical methods alone indicate that frequent and rapid heading adjustments (equivalent to rapid steering wheel adjustments in reality) are dangerous at high speeds. Therefore, a low level of heading-angle fluctuation is conducive to safe driving and stable control of the TTS under high-speed conditions. The experimental results also demonstrate that the TTS-DM method can fully utilize the trailer autoregressive performance of the TTS on straightaways, thereby avoiding additional and frequent heading-angle adjustments. Comparative experiments further verify the effectiveness of the proposed algorithm.

5. Conclusions

This study explores the dual-trajectory planning and the stable control strategy of a tractor-trailer system based on an intelligent engineering application background for agricultural equipment in saline alkali land. Traditional research of TTS typically uses a single path as a reference benchmark. In this context, the inconsistency between the trajectories of the tractor and trailer is often regarded as a system or control error. In fact, the research results show that the motion laws of the tractor and the trailer in the TTS are independent and different. Enforcing consistency between the trajectories of the active and passive vehicles will inevitably compromise system control and stability.

To solve the stability control challenges of the TTS for saline alkali land, a dual-trajectory collaborative prediction algorithm and a lateral stability control method based on the TTS kinematic/dynamic model are proposed. First, we reconstructed the kinematic and dynamic model of the TTS to satisfy the application requirements under both low- and high-speed conditions. Utilizing the system model and an analysis of motion laws, we developed a dual-trajectory collaborative prediction algorithm to generate accurate predictions for the trailer's trajectories. In this manner, the independence of the trajectory between the tractor and trailer was also verified. Subsequently, based on the dual-trajectory collaborative prediction, a lateral stability control algorithm for the TTS was proposed. This control method incorporates a graded control strategy for both low- and high-speed conditions, along with a trailer lateral stability control method. By fully integrating the independent reference track of the trailer with its lateral offset, the control scheme optimizes redundant control, balances the dynamic tracking performance of the tractor, maintains the stationarity of the trailer, and enhances the overall control stability of the system.

The observability and controllability of the underactuated TTS were verified. Based on the control strategy, the TTS-DM method can fully leverage the trailer's autoregressive performance on straightaways, thereby minimizing the need for frequent heading-angle adjustments. This approach addresses the challenge of balancing trailer trajectory tracking

performance with tractor dynamic control stability, which is often a limitation in traditional control methods. Consequently, it provides technical support for the intelligent autonomous navigation of TTS in complex saline alkali land farms.

Our proposed method has several limitations: The ground needs to provide sufficient friction to establish effective external constraints. Overly muddy saline alkali land can alter the friction properties, so the tire parameters and the friction coefficient may need to be re-selected and set. In addition, under high-speed conditions, the preview point of the driver model needs to be slightly farther away, and the on-board upper computer needs to provide sufficient computing power to ensure real-time performance.

Author Contributions: Conceptualization, G.L. and S.Z.; methodology, Y.X. and Z.X.; software, F.X., Z.G., Y.X. and E.F.; validation, Z.X.; formal analysis, F.X. and P.Z.; investigation, L.S.; resources, S.Z. and Z.G.; data curation, Z.X. and Z.G.; writing—original draft preparation, G.L.; writing—review and editing, S.Z. and P.Z.; visualization, F.X. and L.S.; supervision, E.F.; project administration, Y.X.; funding acquisition E.F. All authors have read and agreed to the published version of the manuscript.

Funding: This research was funded by Fundamental Research Program of Shanxi Province: 202203021222063; Fundamental Research Program of Shanxi Province: 202303021222101; Fundamental Research Program of Shanxi Province: 202203021222053.

Institutional Review Board Statement: Not applicable.

Data Availability Statement: The original contributions presented in the study are included in the article.

Conflicts of Interest: Authors Yanyun Xue and Enjie Fan was employed by the company Chongqing Chang'an Wangjiang Industry Group Co., Ltd. The remaining authors declare that the research was conducted in the absence of any commercial or financial relationships that could be construed as a potential conflict of interest.

Appendix A

The tractor-trailer state-space Equation (25) representation and parameter matrix definition:

$$\dot{x} = [A\ B_1\ B_3][x\ \delta_1\ \delta_2]^T$$

where $x = [\lambda_1\ \gamma_1\ \gamma_2\ \Delta\varphi]^T x = [\lambda_1\ \gamma_1\ \gamma_2\ \Delta\varphi]^T$

$$A = Y^{-1}K$$

$$B_1 = Y^{-1}q_1$$

$$B_3 = Y^{-1}q_2$$

$$Y = \begin{bmatrix} y_{11} & I_{Z1} & 0 & 0 \\ y_{21} & y_{22} & y_{23} & y_{24} \\ y_{31} & 0 & I_{Z2} & 0 \\ 0 & 0 & 0 & 1 \end{bmatrix}$$

$$y_{11} = (b_1 + l)m_1 u$$

$$y_{21} = (m_1 + m_2)u$$

$$y_{22} = -(b_1 + l)m_2$$

$$y_{23} = -(a_2 + d)m_2$$

$$y_{24} = m_2 u$$

$$y_{31} = (a_2 + d)m_1 u$$

$$K = \begin{bmatrix} k_{11} & k_{12} & 0 & 0 \\ k_{21} & k_{22} & k_{23} & k_{24} \\ k_{31} & k_{32} & k_{33} & k_{34} \\ 0 & 1 & -1 & 0 \end{bmatrix}$$

$$q_1 = -\begin{bmatrix} (a_1 + b_1 + l)C_1 \\ C_1 \\ (a_2 + d)C_1 \\ 0 \end{bmatrix}$$

$$q_2 = -\begin{bmatrix} 0 \\ C_3 \\ a_2C_3 \\ 0 \end{bmatrix}$$

$$k_{11} = (a_1 + b_1)C_1 + (C_1 + C_2)l$$

$$k_{21} = C_1 + C_2 + C_3 + C_4$$

$$k_{31} = (a_2 + d)(C_1 + C_2) + a_2C_3 - b_2C_4$$

$$k_{12} = \frac{(a_1 + b_1 + l)a_1C_1 - b_1lC_2 - (b_1 + l)m_1u^2}{u}$$

$$k_{22} = \frac{-(b_1 + l)(C_3 + C_4) + a_1C_1 - b_1C_2 - m_1u^2}{u}$$

$$k_{32} = \frac{(a_1C_1 - b_1C_2 - m_1u^2)(a_2 + d) + (b_1 + c)(b_2C_4 - a_2C_3)}{u}$$

$$k_{23} = -\frac{(a_2 + b_2)C_4 + d(C_3 + C_4)}{u} - m_2u$$

$$k_{33} = \frac{(a_2 + d + b_2)C_4 - a_2dC_3}{u}$$

$$k_{24} = C_3 + C_4$$

$$k_{34} = a_2C_3 - b_2C_4$$

References

1. Lee, E.; Kim, T.; Mun, H.S.; Oh, J.H.; Han, S.K. Assessing the extent and severity of the impact on forest soils of two different fully mechanized timber harvesting operations. *Forests* **2024**, *15*, 985. [CrossRef]
2. Zou, L.; Liu, X.; Yuan, J.; Dong, X. Research progress in mechanized harvesting technology and equipment of leafy vegetables. *J. Chin. Agric. Mech.* **2022**, *43*, 15–23.
3. Visser, R.M.; Spinelli, R. Benefits and limitations of winch-assist technology for skidding operations. *Forests* **2023**, *14*, 296. [CrossRef]
4. Li, Y.; Zhang, P.; Yuan, J.; Liu, X. Visual positioning and harvesting path optimization of white asparagus harvesting robot. *Smart Agric.* **2020**, *2*, 65–78.
5. Chang, H.; Han, H.S.; Anderson, N.; Kim, Y.S.; Han, S.K. The cost of forest thinning operations in the western united states: A systematic literature review and new thinning cost model. *J. For.* **2023**, *121*, 193–206. [CrossRef]
6. Li, T.; Huang, S.; Niu, Z.; Hou, J.; Wu, Y.; Li, Y. Optimization and experiment of planting perpendicularity of planetary wheel garlic planter. *Trans. Chin. Soc. Agric. Eng. (Trans. CSAE)* **2020**, *36*, 37–45.
7. Li, J.; Liu, X.; Zou, L.; Yuan, J.; Du, S. Analysis of the interaction between end-effectors, soil and asparagus during a harvesting process based on discrete element method. *Biosyst. Eng.* **2020**, *196*, 127–144. [CrossRef]
8. Kumar, N. Backstepping based intelligent control of tractor-trailer mobile manipulators with wheel slip consideration. *ISA Trans.* **2024**, *153*, 78–95.
9. Shi, M.; Feng, X.; Pan, S.; Song, X.; Jiang, L. A collaborative path planning method for intelligent agricultural machinery based on unmanned aerial vehicles. *Electronics* **2023**, *12*, 3232. [CrossRef]

10. Tang, Y.; Cai, Y.; Liu, Z.; Sun, X.; Chen, L.; Wang, H.; Dong, Z. Research on active trailer steering control strategy of tractor semitrailer under medium-/high-speed conditions. *Actuators* **2024**, *13*, 360. [CrossRef]
11. Ren, H.; Wu, J.; Lin, T.; Yao, Y.; Liu, C. Correction: Ren et al. Research on an Intelligent Agricultural Machinery Unmanned Driving System. Agriculture 2023, *13*, 1907. *Agriculture* **2024**, *14*, 13.
12. Wang, P.; Yue, M.; Yang, L.; Luo, X.; He, J.; Man, Z.; Feng, D.; Liu, S.; Liang, C.; Deng, Y.; et al. Design and test of intelligent farm machinery operation control platform for unmanned farms. *Agronomy* **2024**, *14*, 804. [CrossRef]
13. Murillo, M.; Sánchez, G.; Deniz, N.; Genzelis, L.; Giovanini, L. Improving path-tracking performance of an articulated tractor-trailer system using a non-linear kinematic model. *Comput. Electron. Agric.* **2022**, *196*, 106826. [CrossRef]
14. Wen, H.; Ma, X.; Qin, C.; Chen, H.; Kang, H. Research on path tracking of unmanned spray based on dual control strategy. *Agriculture* **2024**, *14*, 562. [CrossRef]
15. Ahn, Y.; Han, S.; Kim, G.; Huh, K. Slope and mass estimation for semi-trailer tractor considering pitch angle variations. *IEEE Trans. Intell. Veh.* **2024**, *1*, 1–13. [CrossRef]
16. Zhou, Y.; Chung, K.W. Path tracking control of a tractor-trailer wheeled system kinematics with a passive steering angle. *Appl. Math. Model.* **2022**, *109*, 341–357. [CrossRef]
17. Jin, Z.; Wang, C.; Liang, D.; Wang, S.; Ding, Z. Fixed-time consensus for multiple tractor-trailer vehicles with dynamics control: A distributed internal model approach. *IEEE Trans. Intell. Veh.* **2024**, *9*, 656–669. [CrossRef]
18. Wang, D.; Moon, I.; Zhang, R. Multi-trip multi-trailer drop-and-pull container drayage problem. *IEEE Trans. Intell. Transp. Syst.* **2022**, *23*, 19088–19104. [CrossRef]
19. Jin, X.; Liang, J.; Dai, S.L.; Guo, D. Adaptive line-of-sight tracking control for a tractor-trailer vehicle system with multiple constraints. *IEEE Trans. Intell. Transp. Syst.* **2022**, *23*, 11349–11360. [CrossRef]
20. Han, S.; Yoon, K.; Park, G.; Huh, K. Hybrid state observer design for estimating the hitch angles of tractor-multi unit trailer. *IEEE Trans. Intell. Veh.* **2023**, *8*, 1449–1458. [CrossRef]
21. Zhao, C.; Zhu, Y.; Du, Y.; Liao, F.; Chan, C.Y. A novel direct trajectory planning approach based on generative adversarial networks and rapidly-exploring random tree. *IEEE Trans. Intell. Transp. Syst.* **2022**, *23*, 17910–17921. [CrossRef]
22. Han, S.; Yoon, K.; Park, G.; Huh, K. Robust lane keeping control for tractor with multi-unit trailer under parametric uncertainty. *IEEE Trans. Intell. Veh.* **2024**, *9*, 2333–2347. [CrossRef]
23. Chen, K.; Deng, J.; Zhang, W.Z. Kinematic analysis of tractor-trailer mobile robot on a sphere. In Proceedings of the 2023 International Conference on Intelligent Communication and Computer Engineering (ICICCE), Changsha, China, 27–29 December 2023; pp. 121–128.
24. Shojaei, K.; Taghavifar, H. Input-output feedback linearization control of a tractor with n-trailers mechanism considering the path curvature. *Proc. Inst. Mech. Eng. Part C J. Mech. Eng. Sci.* **2022**, *236*, 9700–9715. [CrossRef]
25. Yun, S.H.; Yang, J.G.; Huh, K.S. Development of a narrow passage driving system for semi-trailer tractor by using MPC. *Int. J. Automot. Technol.* **2022**, *23*, 785–791. [CrossRef]
26. DeSantis, R.M. Path-tracking for a tractor-trailer-like robot. *Int. J. Robot. Res.* **1994**, *13*, 533–544. [CrossRef]
27. Bulgakov, V.; Aboltins, A.; Ivanovs, S.; Beloev, H.; Nadykto, V.; Ihnatiev, Y.; Olt, J. Theory of movement of machine-tractor unit with trailer haulm harvester machine. *Appl. Sci.* **2022**, *12*, 3901. [CrossRef]
28. Hellander, A.; Bergman, K.; Axehill, D. On Integrated optimal task and motion planning for a tractor-trailer rearrangement problem. In Proceedings of the 2023 62nd IEEE Conference on Decision and Control (CDC), Singapore, 13–15 December 2023; pp. 6116–6123.
29. Zhao, H.; Chen, W.; Zhou, S.; Zheng, F.; Liu, Y.H. Localization and motion planning of industrial tractor–trailers vehicles. *IEEE Trans. Control Syst. Technol.* **2023**, *31*, 2928–2936. [CrossRef]
30. Lu, E.; Zhao, X.; Ma, Z.; Xu, L.; Liu, Y. Robust leader-follower control for cooperative harvesting operation of a tractor-trailer and a combine harvester considering confined space. *IEEE Trans. Intell. Transp. Syst.* **2024**, *25*, 17689–17701. [CrossRef]
31. Liu, J.; Han, W.; Peng, H.; Wang, X. Trajectory planning and tracking control for towed carrier aircraft system. *Aerosp. Sci. Technol.* **2019**, *84*, 830–838. [CrossRef]
32. Ruan, X.; Huang, Y.; Wang, Y.; Fu, Z.; Xiong, L.; Yu, Z. An efficient trajectory-planning method with a reconfigurable model for any tractor trailer vehicle. *IEEE Trans. Transp. Electrif.* **2023**, *9*, 3360–3374. [CrossRef]
33. Jin, X.; Dai, S.L.; Liang, J. Adaptive constrained formation-tracking control for a tractor-trailer mobile robot team with multiple constraints. *IEEE Trans. Autom. Control* **2023**, *68*, 1700–1707. [CrossRef]
34. Manav, A.C.; Lazoglu, I.; Aydemir, E. Adaptive path following control for autonomous semi-trailer docking. *IEEE Trans. Veh. Technol.* **2022**, *71*, 69–85. [CrossRef]
35. Widyotriatmo, A.; Nazaruddin, Y.Y.; Putrantob, M.R.F.; Ardhi, R. Forward and backward motions path following controls of a tractor-trailer with references on the head-tractor and on the trailer. *ISA Trans.* **2020**, *105*, 349–366. [CrossRef]
36. Ljungqvist, O.; Evestedt, N.; Axehill, D.; Cirillo, M.; Pettersson, H. A path planning and path following control framework for a general 2-trailer with a car-like tractor. *J. Field Robot.* **2019**, *36*, 1345–1377. [CrossRef]

37. Peng, H.; Shi, B.; Song, J.; Wang, X. A symplectic method for trajectory planning of general tractor-trailer systems. *Appl. Math. Model.* **2023**, *114*, 205–229. [CrossRef]
38. Ito, N.; Okuda, H.; Suzuki, T. Configuration-aware model predictive motion planning for Tractor–Trailer Mobile Robot. *Adv. Robot.* **2023**, *37*, 329–343. [CrossRef]
39. Lei, G.; Zheng, Y. Research on collaborative trajectory planning algorithm based on Tractor-Trailer Wheeled System. *IEEE Access* **2022**, *10*, 64209–64221. [CrossRef]
40. Zhuang, J. *Automotive Tire Science*, 1st ed.; Beijing Institute of Technology Press: Beijing, China, 1995; pp. 186–229.